New Families of Fourier Eigenfunctions for Steerable Filtering

Papari, Giuseppe; Campisi, Patrizio; Petkov, Nicolai

Published in:
Ieee transactions on image processing

DOI:
10.1109/TIP.2011.2179060

Publication date:
2012

New Families of Fourier Eigenfunctions for Steerable Filtering

Giuseppe Papari, *Member, IEEE*, Patrizio Campisi, *Senior Member, IEEE*, and Nicolai Petkov

***Abstract*—A new diadic family of eigenfunctions of the 2-D Fourier transform has been discovered. Specifically, new wavelets are derived by steering the elongated Hermite–Gauss filters with respect to rotations, thus obtaining a natural generalization of the Laguerre–Gauss harmonics. Interestingly, these functions are also proportional to their 2-D Fourier transform. Their analytical expression is provided in a compact and treatable form, by means of a new ad hoc matrix notation in which the cases of even and odd orders of the Hermite polynomials are unified. Moreover, these functions can be efficiently implemented by means of a recursive formula that is derived in this paper. The proposed filters are applied to the problem of gradient estimation to improve the theoretical Canny tradeoff of position accuracy versus noise rejection that occurs in edge detection. Experimental results show considerable improvements in using the new wavelets over both isotropic Gaussian derivatives and other elongated steerable filters more recently introduced. Finally, being the proposed wavelets a set of Fourier eigenfunctions, they can be of interest in other fields of science, such as optics and quantum mechanics.**

***Index Terms*—Filtering, series expansion methods, wavelets and fractals.**

NOTATION

$\mathbf{r}$	Vector in the 2-D spatial domain.
$\boldsymbol{\omega}$	Vector in the 2-D frequency domain.
(x, y)	Cartesian coordinates of $\mathbf{r}$.
(r, θ)	Polar coordinates of $\mathbf{r}$.
(ξ, η)	Cartesian coordinates of $\boldsymbol{\omega}$.
(ρ, ϕ)	Polar coordinates of $\boldsymbol{\omega}$.
$\tilde{x}(\boldsymbol{\omega})=\mathcal{F}_{2D}\{x(\mathbf{r})\}$ $x(\mathbf{r})\xrightarrow{\mathcal{F}_{2D}}\tilde{x}(\boldsymbol{\omega})$	2-D Fourier transform.

Manuscript received April 27, 2011; revised September 06, 2011; accepted November 08, 2011. Date of publication December 09, 2011; date of current version May 11, 2012. The associate editor coordinating the review of this manuscript and approving it for publication was Prof. Marios S. Pattichis.

G. Papari was with Johann Bernoulli Institute of Mathematics and Computer Science, University of Groningen, 9700 AK Groningen, The Netherlands. He is now with the National Institute of Research in Informatics and Automatics, Rocquencourt, BP 105-78153 Le Chesnay Cedex, France.

P. Campisi is with the Dipartimento di Elettronica Applicata, Universita' degli Studi Roma Tre, 00146 Roma, Italy.

N. Petkov is with Johann Bernoulli Institute of Mathematics and Computing Science, University of Groningen, Groningen, 9700 AK Groningen, The Netherlands.

Color versions of one or more of the figures in this paper are available online at http://ieeexplore.ieee.org.

Digital Object Identifier 10.1109/TIP.2011.2179060

I. INTRODUCTION

WAVELETS play a central role in pattern recognition [1]. An important family of wavelets is given by the Hermite–Gauss filters (HGFs) [2], [3], which are defined as the product of Hermite polynomials with an isotropic Gaussian term. HGFs have nice mathematical properties: they are closely related to the Gaussian derivatives, they are very close to the optimal for feature detection [4], and they have interesting causality properties for regularization in the scale space [5], [6]. Due to these features, HGFs find many applications in image analysis, such as local features detection [7], video denoising [8], and astronomical image compression [9], [10]. Moreover, they form a complete set of orthogonal eigenfunctions of the 2-D Fourier transform, which makes them appealing for other fields of science as well, such as optics and quantum mechanics.

HGFs are *steerable* w.r.t. rotations, i.e., any rotated HGF can be expressed as a linear combination of a finite number of fixed *steering functions*, with coefficients that depend on the rotation angle only. Steerability makes HGFs interesting for analyzing oriented features, such as edges and ridges, because the convolution of an image with any rotated HGF can be exactly and efficiently evaluated after convolving the input image with the steering bases. The steering functions of the HGFs are known in the literature as Laguerre–Gauss harmonics and are expressed, in polar coordinates, as the product of a Gaussian term with Laguerre polynomials and a complex exponential [2], [11]. The concept of steerability has been successfully applied in several areas of image processing, such as orientation-selective feature detection [11]–[18], nonlinear filtering [19], texture modeling [20], denoising [21], [22], invariance theory [23], and wavelets theory [24], [25]. More details about steerable filters are given in Section II-A.

An intrinsic limit of the HGFs is that the same amount of smoothing is made in all directions, due to the isotropic Gaussian factor. This results in a theoretical compromise between noise rejection and position accuracy, as illustrated in Fig. 1 for the case of edge detection. Specifically, let us suppose we want to detect a double-edge corrupted by noise, as shown in Fig. 1(a). When isotropic kernels of different size are used [see Fig. 1(b) and (c)], either low noise rejection or low position accuracy is obtained [see Fig. 1(d) and (e), respectively]. In particular, at large scales, most of the noise is rejected, but the uncertainty on the edge position is so high that the two edges are no longer resolvable [see Fig. 1(e)]. In contrast, if an elongated convolution kernel is employed [see Fig. 1(f)], both high regularization and high localization can be achieved at the same time [see Fig. 1(g)].

Another advantage of using elongated filters is that they are more selective w.r.t. orientations. An example is shown

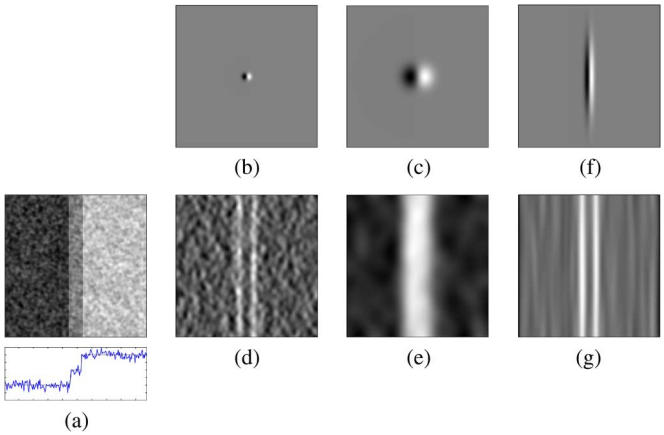

Fig. 1. Improvement in the tradeoff of noise rejection versus edge position accuracy that is carried out by elongated HGF w.r.t. isotropic ones. (a) Noisy double edge to be detected. [(b) and (c)] x-derivative of two nonelongated Gaussian kernels, for two different values of the scale parameter. [(d) and (e)] Convolution of the double edge shown in (a) with the isotropic kernels of (b) and (c), respectively. (f) An elongated convolution kernel and (g) the output of the convolution. Nonelongated filters result in either poor noise rejection or little accuracy in the position of the detected edges. In contrast, elongated kernels allow to achieve both good noise rejection and good edge accuracy.

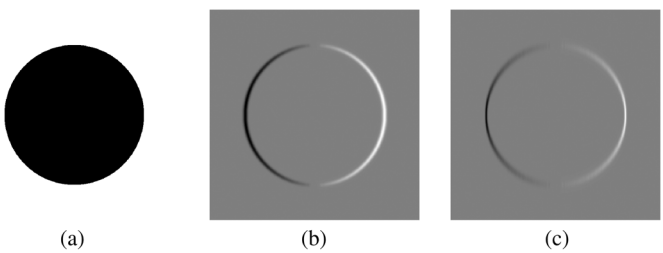

Fig. 2. Improvement in orientation selectivity that is carried out by the elongated HGF w.r.t. the isotropic ones. (a) Synthetic image and the result of the convolution with the x-derivative of (b) nonelongated and (c) elongated Gaussian kernels, respectively. The elongated kernel results in a higher orientation selectivity, as the response is high only for those edges whose orientation is very close to vertical.

in Fig. 2, for the problem of detecting vertical edges. For the synthetic input image of Fig. 2(a), the output of the convolution with both isotropic and elongated edge-detection kernels is shown in Fig. 2(b) and (c). As desired, the response to the elongated filter is high only for vertical edges. In contrast, for the nonelongated case, the response is high for a wide range of orientations other than the vertical one.

A consequence of high orientation selectivity is that different types of oriented features can be distinguished from each other and from noise by analyzing the so-called *angular signature* of a local pattern around each pixel of the input image [26]. Given a convolution kernel, the angular signature of an image w.r.t. that kernel is the inner product between the image and the rotated kernel, as a function of the rotation angle. Examples of the angular signatures are illustrated in Fig. 3. Specifically, the angular signatures of an edge, a corner, and noise, w.r.t. both elongated and isotropic convolution kernels, are shown as polar diagrams. As it is evident, the signatures w.r.t. the elongated HGFs have different shapes for each pattern, whereas for the nonelongated case, they are always circular. Therefore, elongated filters have higher discrimination power than isotropic ones in the angular domain.

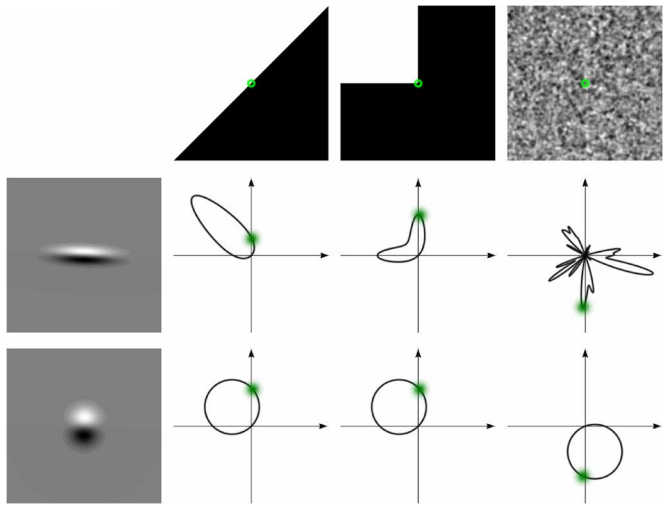

Fig. 3. Illustration of the concept of *angular signature*. Top row: Three local patterns (edge, corner, and noise). Middle row: First derivative of an elongated Gaussian and its inner product with each local patterns as a function of the orientation (signature), represented as a polar diagram. Bottom row: Same for an isotropic kernel. An elongated convolution kernel results in a more informative signature, as different patterns result in different shaped signatures, thus increasing discriminative power w.r.t. the isotropic case.

A limitation of the elongated HGFs is that, unlike isotropic HGFs, they are not steerable w.r.t. rotations. In other words, the family of rotated elongated HGFs needs an infinite set of steering functions to be exactly represented. Therefore, we are interested in finding steerable convolution kernels, which best approximate the elongated HGF. A well-established framework to achieve this goal is the singular value decomposition (SVD) [13], [27], [28], which leads to the minimum square error steerable approximation of a given kernel and produces orthogonal steering functions. However, the SVD only provides numerical approximations for the steering bases, thus allowing no theoretical study of their properties. In particular, at the current state of the art, the steering functions of the elongated HGF are known only as numerical approximations and for a few orders only.

On the contrary, we are interested in analytical expressions for the general case. In this paper, the steering functions that best approximate the elongated HGFs are derived analytically for any order. While the mathematical expressions are rather complex, we introduce a matrix notation in which the new wavelets are expressed in a very compact form, and the cases of odd and even orders of the Hermite polynomials are unified. The matrix notation makes the new steering functions more treatable and facilitates a theoretical study of their properties. In particular, we derive a convenient recursive implementation of the new steering functions, and we demonstrate that they give rise to a new dyadic family of eigenfunctions of the 2-D Fourier transform. This result is not trivial because the elongated HGFs, from which the new steering functions are derived, are not Fourier eigenfunctions. As a proof of concept, we also apply the introduced wavelets to gradient estimation for edge detection. Our experimental results, although interesting and promising, are only illustrative, as the main focus of this paper is theoretical.

The rest of this paper is organized as follows: After a short review on steerable filters and elongated HGFs in Section II, we provide a closed form for the related steering functions, along

Fig. 4. (a) Basic convolution kernel (vertical line detector) and the result of several geometrical transformation: (a) rotation, (b) isotropic, and (c) anisotropic scaling, and (d) curvature deformation.

with some mathematical properties, in Section III and compute their Fourier transforms in Section IV. Finally, we show an application of the new filters to gradient estimation in Section V, and we draw conclusions in Section VI.

II. Background

In this section, background on steerable filtering (see Section II-A) and elongated HGFs (see Section II-B) is provided.

A. Steerable Filters

Let $T(\mathbf{r})$ be a convolution kernel, and let $\mathcal{T}_{\boldsymbol{\gamma}} : \mathbb{R}^2 \mapsto \mathbb{R}^2$ be a geometric transformation that depends on the P-dimensional parameter $\boldsymbol{\gamma} \triangleq [\gamma_1, \ldots, \gamma_P]^\top$. Moreover, let us consider the family of filters $F(\mathbf{r};\boldsymbol{\gamma}) \triangleq T[\mathcal{T}_{\boldsymbol{\gamma}}(\mathbf{r})]$, which are obtained by applying transformation $\mathcal{T}_{\boldsymbol{\gamma}}$ to $T(\mathbf{r})$. This is illustrated in Fig. 4 for several geometric transformations, in which $T(\mathbf{r})$ is the second x-derivative of a Gaussian [see Fig. 4(a)] and transformations $\mathcal{T}_{\boldsymbol{\gamma}}$ are rotation, isotropic, and anisotropic scalings, and a curvature deformation, respectively [see 4(b)–(e), respectively]. In image processing, deformed filters are deployed in several contexts to detect features that depend on several parameters, such as orientation, scale, elongation, and curvature.

A widespread approach to implement the convolution of an input image $I(\mathbf{r})$ with the family of filters $F(\mathbf{r};\boldsymbol{\gamma})$ is to discretize parameter $\boldsymbol{\gamma}$ and to convolve the image with the resulting filters. Good examples of practical situations in which such a discretization is widely used are Gabor filtering and scale space analysis. Although such an approach can be straightforwardly implemented, it introduces a discretization error, it might require a large number of convolutions, and inelegant methods are applied to collapse the outputs of many convolutions into a single quantity.

A different solution introduced in [29], called *steerable filtering*, consists in expanding the whole family $F(\mathbf{r};\boldsymbol{\gamma})$ into a superposition of N *steering functions* $V^s(\mathbf{r})$ independent of $\boldsymbol{\gamma}$, $s = 1, \ldots, N$, with *steering coefficients* $a^s(\boldsymbol{\gamma})$, i.e.,

$$F(\mathbf{r},\boldsymbol{\gamma}) = \sum_{s=1}^{N} a^s(\boldsymbol{\gamma}) V^s(\mathbf{r}). \tag{1}$$

A convolution kernel $T(\mathbf{r})$ is said to be *steerable* w.r.t. the geometric transformation $\mathcal{T}_{\boldsymbol{\gamma}}$ when such a factorization is possible with a finite number of terms. In such a case, the output of convolution $Y(\mathbf{r},\boldsymbol{\gamma}) \triangleq I(\mathbf{r}) \star F(\mathbf{r},\boldsymbol{\gamma})$ of an image $I(\mathbf{r})$ with $F(\mathbf{r},\boldsymbol{\gamma})$ can be exactly evaluated for any value of $\boldsymbol{\gamma}$ by convolving $I(\mathbf{r})$ with the steering functions $V^s(\mathbf{r})$, i.e.,

$$I(\mathbf{r}) \star F(\mathbf{r},\boldsymbol{\gamma}) = \sum_{s=1}^{N} a^s(\boldsymbol{\gamma}) \left[I(\mathbf{r}) \star V^s(\mathbf{r}) \right]. \tag{2}$$

Because of the linearity of convolution, no discretization of $\boldsymbol{\gamma}$ is needed, and the whole family $F(\mathbf{r};\boldsymbol{\gamma})$ is thought as a continuum in the domain of $\boldsymbol{\gamma}$. While both frameworks—discretization of $\boldsymbol{\gamma}$ and steerable filtering—lead to the convolution of the input image with a filter bank, practice shows that steerable filters require a smaller number of convolutions for the same accuracy [30]. Moreover, steerable filters allow exact evaluation of integrals and derivatives of $I(\mathbf{r}) \star F(\mathbf{r},\boldsymbol{\gamma})$ w.r.t. $\boldsymbol{\gamma}$ by integrating or differentiating coefficients $a^s(\boldsymbol{\gamma})$ in (2). This would not be possible after discretizing $\boldsymbol{\gamma}$.

An important task in steerable filtering is finding the steering bases for which factorization (1) is possible and requires the minimum number of terms. Several techniques have been proposed for this purpose, which are based on the Lie group theory (LGT) [31] and the SVD of a matrix [13], [27], [28].

In LGT approaches, eigenfunction $\Psi(\mathbf{r})$ of a geometric deformation $\mathcal{T}_{\boldsymbol{\gamma}}$ is a function that is invariant w.r.t. $\mathcal{T}_{\boldsymbol{\gamma}}$, apart for a multiplicative factor $\lambda(\boldsymbol{\gamma})$, i.e.,

$$\Psi\left[\mathcal{T}_{\boldsymbol{\gamma}}(\mathbf{r})\right] = \lambda(\boldsymbol{\gamma}) \Psi(\mathbf{r}). \tag{3}$$

By comparing (3) with (1), it is evident that any linear combination of an eigenfunction $\Psi^s(\mathbf{r})$ of $\mathcal{T}_{\boldsymbol{\gamma}}$ is steerable w.r.t. $\mathcal{T}_{\boldsymbol{\gamma}}$, where the steering functions coincide with eigenfunctions $\Psi^s(\mathbf{r})$. In [31], orthogonal eigenfunctions are analytically expressed for some simple geometrical transformations, such as translation, rotation, and scaling. The resulting steering functions are also optimal in a least-squared-error sense. LGT allows finding the general form of the steering functions $V^s(\mathbf{r})$ independently of the particular convolution kernel to be steered. Moreover, the eigenfunctions being orthonormal, the steering coefficients $a^s(\boldsymbol{\gamma})$ can be computed by standard orthogonal projection. However, LGT often results in a continuum spectrum of eigenfunctions, thus making factorization (1) impossible with a finite number of terms. A solution would be discretizing such a spectrum, but then the completeness and the optimality of eigenfunctions $\Psi^s(\mathbf{r})$ would be lost.

A different approach, which overcomes these limitations, was proposed in [13], based on the SVD decomposition of matrices. The idea is to find the steering functions $V^s(\mathbf{r})$ and the steering coefficients $a^s(\boldsymbol{\gamma})$ directly, by minimizing the error of approximating $F(\mathbf{r};\boldsymbol{\gamma})$ with expansion (1), i.e.,

$$\min_{V^s(\mathbf{r}),a^s(\boldsymbol{\gamma})} \left\| F(\mathbf{r};\boldsymbol{\gamma}) - \sum_{s=1}^{N} a^s(\boldsymbol{\gamma}) V^s(\mathbf{r}) \right\|. \tag{4}$$

Two different norms are considered in [13], and it is proved that they lead to the same result. In particular, it can be proven that the basis functions $V^s(\mathbf{r})$ that minimize (4) are solutions $\Psi^s(\mathbf{r})$ of the following eigenanalysis problem:

$$\int_{\mathbb{R}^2} \Phi(\mathbf{r},\zeta) \Psi(\zeta) \mathrm{d}\zeta = \lambda \Psi(\mathbf{r}) \tag{5}$$

with

$$\Phi(\mathbf{r},\zeta) \triangleq \int_{\Omega \subseteq \mathbb{R}^P} F(\mathbf{r};\boldsymbol{\gamma}) F(\zeta;\boldsymbol{\gamma}) \mathrm{d}\boldsymbol{\gamma}. \tag{6}$$

In practice, (5) is hard to exactly solve, except for a few simple cases. It is numerically solved by performing the SVD

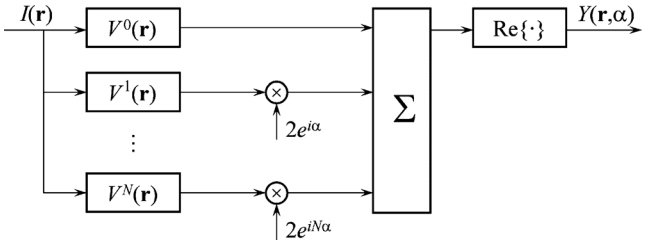

Fig. 5. Implementation of the convolution of an image with a steerable kernel w.r.t. rotations.

of a matrix whose entries are the values of $F(\mathbf{r};\boldsymbol{\gamma})$ for discrete values of $\mathbf{r}$ and $\boldsymbol{\gamma}$. Some extensions of this technique have been proposed in several directions, such as constraining the steering functions to be separable in the x and y coordinates [32], or reducing the computational complexity when the dimensionality of $\boldsymbol{\gamma}$ is high [28].

In general, SVD ensures a discrete set of orthogonal steering functions, thus overcoming the main limitation of LGT. However, the steering functions are rarely expressed analytically and their optimality only holds for the specific convolution kernels for which they are designed. Moreover, because the dependence of coefficients $a^s(\boldsymbol{\gamma})$ on $\boldsymbol{\gamma}$ is also numerically given, the evaluation of $Y(\mathbf{r},\boldsymbol{\gamma})$ by means of (2) is no longer exact for every value of $\boldsymbol{\gamma}$, as it is in the LGT case.

In this paper, we focus on the case in which the geometric transformation $\mathcal{T}_{\boldsymbol{\gamma}}$ is a rotation with parameter $\boldsymbol{\gamma}$ equal to the rotation angle α. In other words, we have $F(\mathbf{r},\alpha) = T(R_\alpha \mathbf{r})$, where R_α is the rotation matrix with angle α. In this case, both LGT and SVD lead to the result that the steering functions $V^s(\mathbf{r})$ are *circular harmonic functions* (CHFs). In other words, in polar coordinates, they factorize as the product of a radial term $U^s(r)$ with a complex exponential $e^{is\theta}$, i.e.,

$$V^s(r,\theta) = U^s(r)e^{is\theta}. \tag{7}$$

Term $U^s(r)$ coincides with the sth coefficient of the Fourier expansion of the steered filter $T(r,\theta)$ w.r.t. θ.

It is straightforward to see that every CHF $V^s(\mathbf{r})$ is an eigenfunction of the rotation operator R_α, with eigenvalue $e^{is\alpha}$, i.e.,

$$V^s(R_\alpha \mathbf{r}) = V^s(r,\theta+\alpha) = U^s(r)e^{is(\theta+\alpha)} = e^{is\alpha}V^s(\mathbf{r}). \tag{8}$$

Therefore, when a given convolution kernel $T(\mathbf{r})$ is expressed as a sum of appropriate CHF $V^s(\mathbf{r})$, i.e., $T(r,\theta) = \sum_{s=-N}^{N} U^s(r)e^{is\theta}$, we have

$$T(R_\alpha \mathbf{r}) = \sum_{s=-N}^{N} e^{is\alpha}V^s(\mathbf{r}). \tag{9}$$

By comparing this equation with (1), we conclude that filter $T(\mathbf{r})$ is steerable w.r.t. rotations if it can be expressed as a linear superposition of CHF. Moreover, the steering coefficients are $a^s(\alpha) = e^{is\alpha}$ for every convolution kernel.

In practical implementations, CHFs $V^s(\mathbf{r})$ are considered for $s \geq 0$ only, due to equality $V^{-s}(\mathbf{r}) = \overline{V}^s(\mathbf{r})$, where $\overline{z}$ denotes the complex conjugate of a complex number z. This reduces the computational complexity by a factor of 2 w.r.t. (9). The implementation scheme is shown in Fig. 5.

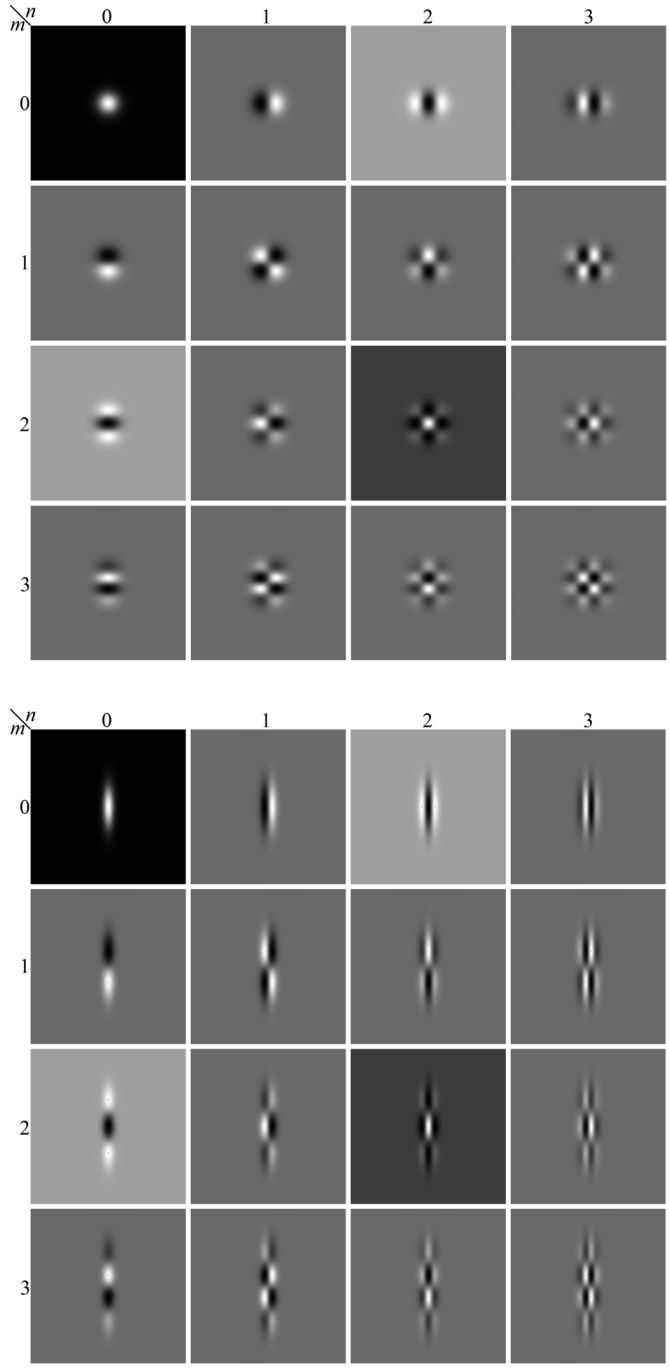

Fig. 6. Examples of HGF of several orders, from $(m,n) = (0,0)$ to $(m,n) = (3,3)$, both for the isotropic $(\lambda = 1)$ and elongated $(\lambda = 2)$ cases.

B. HGFs and Elongated HGFs

Elongated HGFs $H_{m,n}(x,y;\lambda)$ are defined as follows:

$$H_{m,n}(x,y;\lambda) \triangleq H_m(\lambda x)H_n(\lambda^{-1}y)e^{-\frac{(\lambda x)^2+(\lambda^{-1}y)^2}{2}} \tag{10}$$

where $H_p(x) \triangleq (-1)^p e^{x^2}(\mathrm{d}/\mathrm{d}x)^p e^{-x^2}$ is the pth order Hermite polynomial and the parameter $\lambda > 0$ controls elongation. For $\lambda = 1$, the Gaussian term becomes isotropic, and these filters reduce to the classical HGFs. Examples of both isotropic and elongated HGFs of different orders are shown in Fig. 6.

The Fourier transform of an elongated HGF is an elongated HGF, with λ replaced by λ^{-1}, i.e.,

$$H_{m,n}(x,y;\lambda) \xrightarrow{\mathcal{F}_{2D}} i^{m+n} H_{m,n}(\xi,\eta;\lambda^{-1}). \quad (11)$$

For $\lambda = 1$, this identity reduces to the well-known result that isotropic HGFs are eigenfunctions of the 2-D Fourier transform.

We are interested in the performance of these convolution kernels for oriented-feature detection in terms of noise rejection and localization. Specifically, let $K(x,y)$ be a convolution kernel that detects a certain oriented feature (edge, ridge, corner, etc.). We will assume for the moment that the concerned feature is vertically oriented. The following facts are well known.

1) The convolution kernel $(1/\sigma^2)K(x/\sigma, y/\sigma)$, where $\sigma > 0$ is the scale parameter, detects the same feature as $K(x,y)$, at scale σ. Noise rejection, defined in terms of the standard peak signal-to-noise ratio (SNR), is proportional to σ^2. Uncertainty in the position of the concerned feature, defined as the value of the first zero of the autocorrelation of $(1/\sigma^2)K(x/\sigma, y/\sigma)$ in the orthogonal direction to the orientation of the concerned feature (x direction in this case), is proportional to σ. Therefore, isotropic scaling of a given kernel not only improves the performance in terms of noise rejection, but it also introduces a larger localization error.
2) The convolution kernel $(1/\sigma^2)K(\lambda x/\sigma, \lambda^{-1}y/\sigma)$, where $\lambda > 0$ is the elongation parameter, determines the same feature as $K(x,y)$. It is easy to prove that noise rejection is proportional to $(\lambda^{-1}\sigma)(\lambda\sigma) = \sigma^2$. As we see, noise rejection does not depend on λ but on σ only. In fact, the amount of smoothing of these filters is proportional to $\lambda^{-1}\sigma$ along the x axis and to $\lambda\sigma$ along the y-axis; thus, the product of the two does not depend on λ. In contrast, it is easily proven that the localization error, as previously defined, is proportional to $\lambda^{-1}\sigma$.

Therefore, it is possible to increase localization accuracy without affecting noise rejection by increasing λ. This motivates our interest for elongated HGF over the isotropic case.

To detect features of any orientation, rotated kernels should be considered. If the elongated HGFs were steerable, this could be efficiently done by means of (2), as described in Section II-A. However, they are exactly steerable for $\lambda = 1$ only, for which the following expansion holds:

$$H_{m,n}(r\cos\theta, r\sin\theta; \lambda = 1) = \sum_{s=-(m+n)}^{m+n} C_{m,n}^{s} e^{-\frac{r^2}{2}} r^s L_{\frac{m+n-s}{2}}^{|s|}(r^2) e^{is\theta} \quad (12)$$

where $L_p^r(u) \triangleq (u^{-p}e^u/r!)(\mathrm{d}/\mathrm{d}u)^r(e^{-u}u^{r+p})$ are the associate Laguerre polynomials and coefficients $C_{m,n}^s$ have a complicated expression that depends on the parity of m and n (see [2] for more details). It can be proven that functions $\mathcal{L}_p^s(r,\theta) \triangleq e^{-(r^2/2)} r^s L_p^{|s|}(r^2) e^{is\theta}$, known as *Laguerre–Gauss harmonics*, are also an orthogonal and complete set of eigenfunctions of the 2-D Fourier transform. The latter property is not surprising when considering that they are the steering coefficients of the isotropic HGF, which are Fourier eigenfunctions as well.

The contribution of this paper is the generalization of (12) to the case of any value of λ and the study of the mathematical properties of the resulting steering functions.

III. Closed Form of the Steering Functions

In this section, we derive a closed form of the steering functions $V^s(\mathbf{r})$ defined in (1). We first deal with the general case by introducing an ad hoc matrix notation in Section III-A, then the case of elongated HGFs is tackled in Section III-B. A recursive formula is eventually derived in Section III-C.

A. General Case

Let $\mathbf{U}(r) \triangleq \{U^s(r)\}_{s=-\infty}^{\infty}$ be an unlimited vector whose components are the radial parts of the steering functions $V^s(\mathbf{r})$ of a given template $T(\mathbf{r})$. We denote with $\mathcal{S}$ a *shifting matrix*, which is defined such that $\{\mathcal{S}\mathbf{a}\}^s = \{\mathbf{a}\}^{s+1}$ for every vector $\mathbf{a}$, where $\{\mathbf{a}\}^s$ denotes the sth component of $\mathbf{a}$. Matrix $\mathcal{S}$ has an unlimited number of elements. In general, operations with infinite matrices are expressed in terms of an infinite series; therefore, convergence problems may occur. However, since matrix $\mathcal{S}$ has only one nonzero element per row, convergence is trivially guaranteed and allows manipulating unlimited matrices with the ordinary algebraic rules. In particular, it is easy to show that the kth power of $\mathcal{S}$ produces a shift of k positions, i.e., $\{\mathcal{S}^k\mathbf{a}\}^s = \{\mathbf{a}\}^{s+k}$.

Let us define

$$\mathcal{R} \triangleq \frac{\mathcal{S}^{-1} + \mathcal{S}}{2} \qquad I \triangleq \frac{\mathcal{S}^{-1} - \mathcal{S}}{2i} \quad (13)$$

and $\boldsymbol{\delta}$ is the discrete time pulse, i.e.,

$$\{\boldsymbol{\delta}\}^s \triangleq \begin{cases} 1, & s = 0 \\ 0, & s \neq 0 \end{cases}. \quad (14)$$

This notation is particularly convenient to manipulate the Fourier series. In particular, given a periodic function $x(\theta)$ that can be expanded in the Fourier series with coefficients $\mathbf{x} \triangleq \{x_s\}_{s=-\infty}^{\infty}$, i.e.,

$$x(\theta) \xrightarrow{\mathcal{F}} \mathbf{x} \quad (15)$$

functions $x(\theta)\cos\theta$ and $x(\theta)\sin\theta$ admit the following expansions:

$$\begin{aligned} x(\theta)\cos\theta &\xrightarrow{\mathcal{F}} \left\{\frac{x^{s+1} + x^{s-1}}{2}\right\}_{s=-\infty}^{\infty} = \mathcal{R}\mathbf{x} \\ x(\theta)\sin\theta &\xrightarrow{\mathcal{F}} \left\{\frac{x^{s+1} - x^{s-1}}{2i}\right\}_{s=-\infty}^{\infty} = I\mathbf{x}. \end{aligned} \quad (16)$$

Moreover, by reiterating (16) m and n times, respectively, we get the following identities:

$$\begin{aligned} x(\theta)\cos^m\theta &\xrightarrow{\mathcal{F}} \mathcal{R}^m\mathbf{x} \\ x(\theta)\sin^n\theta &\xrightarrow{\mathcal{F}} I^n\mathbf{x} \\ x(\theta)\cos^m\theta\sin^n\theta &\xrightarrow{\mathcal{F}} \mathcal{R}^m I^n\mathbf{x}. \end{aligned} \quad (17)$$

Theorem 1: Let $T(x,y)$ be an analytic function. Then, the following result holds:

$$\mathbf{U}(r) = T(r\mathcal{R}, rI)\boldsymbol{\delta}. \tag{18}$$

In other words, function $\mathbf{U}(r)$ has the same analytical expression of $T(x,y)$, where the spatial coordinates x and y are replaced with matrices $r\mathcal{R}$ and rI, respectively.

Proof: By definition, $\mathbf{U}(r)$ is given by the following integral:

$$\mathbf{U}(r) = \frac{1}{2\pi}\int_0^{2\pi} T(r\cos\theta, r\sin\theta)e^{-i\mathbf{s}\theta}\mathrm{d}\theta \tag{19}$$

with $\mathbf{s} \triangleq \{\ldots,-2,-1,0,1,2,\ldots\}$.

By expanding $T(x,y)$ into a Taylor series, i.e., $T(x,y) = \sum_{m,n} t_{m,n}x^m y^n$, we get

$$\mathbf{U}(r) = \sum_{m,n} t_{m,n} r^{m+n}\left(\frac{1}{2\pi}\int_0^{2\pi}\cos^m\theta\sin^n\theta e^{i\mathbf{s}\theta}\mathrm{d}\theta\right). \tag{20}$$

This integral can be evaluated by means of the third equation in (17), in which we plug $x(\theta)=1$, thus having $\mathbf{x}=\boldsymbol{\delta}$. Specifically, we have

$$\frac{1}{2\pi}\int_0^{2\pi}\cos^m\theta\sin^n\theta e^{i\mathbf{s}\theta}\mathrm{d}\theta = \mathcal{R}^m I^n\boldsymbol{\delta} \tag{21}$$

thus obtaining

$$\mathbf{U}(r) = \sum_{m,n} t_{m,n} r^{m+n}\mathcal{R}^m I^n\boldsymbol{\delta} = T(r\mathcal{R}, rI)\boldsymbol{\delta}. \tag{22}$$

■

B. Elongated HGFs

Equation (18) is simple and elegant, but in general, it is difficult to use, as it may require evaluating a transcendent function of the infinite matrices $r\mathcal{R}$ and rI. A more usable expression is hereby derived for the elongated HGFs.

Theorem 2: The radial part $\mathbf{U}_{m,n}(r,\lambda)$ of the steering bases of the elongated HGFs is given by

$$\mathbf{U}_{m,n}(r;\lambda) = e^{-\alpha r^2}H_m(\lambda r\mathcal{R})H_n(\lambda^{-1}rI)\mathbf{I}(\beta r^2) \tag{23}$$

with

$$\mathbf{I}(z) \triangleq \{\ldots,0,I_{-1}(z),0,I_0(z),0,I_1(z),0,\ldots\} \tag{24}$$

with $I_s(z)$ being the sth-order modified Bessel function of the first type and

$$\alpha \triangleq (\lambda^{-2}+\lambda^2)/4 \qquad \beta \triangleq (\lambda^{-2}-\lambda^2)/4. \tag{25}$$

Proof: By using (18) into (10), we have

$$\mathbf{U}_{m,n}(r;\lambda) = H_m(\lambda r\mathcal{R})H_n(\lambda^{-1}rI)\mathbf{Z}(r;\lambda) \tag{26}$$

with

$$\mathbf{Z}(r;\lambda) \triangleq e^{-\frac{(\lambda r\mathcal{R})^2+(\lambda^{-1}rI)^2}{2}}\boldsymbol{\delta}. \tag{27}$$

By plugging (13) into (27) and using (25), term $\mathbf{Z}(r;\lambda)$ can be written as

$$\mathbf{Z}(r;\lambda) = e^{-\frac{\alpha r^2}{2}}e^{\beta r^2(\mathcal{S}^2+\mathcal{S}^{-2})}\boldsymbol{\delta}. \tag{28}$$

Then, by using the well-known expansions $e^u = \sum_{n=0}^{\infty}(u^n/n!)$ and $(u+v)^n = \sum_{k=0}^{n}\binom{n}{k}v^k u^{n-k}$, $\mathbf{Z}(r;\lambda)$ can be rearranged as

$$\begin{aligned}\mathbf{Z}(r;\lambda) &= e^{-\alpha r^2}\sum_{n=0}^{\infty}\left(\frac{\beta r^2}{2}\right)^n\frac{(\mathcal{S}^2+\mathcal{S}^{-2})^n}{n!}\boldsymbol{\delta}\\ &= e^{-\alpha r^2}\sum_{n=0}^{\infty}\sum_{k=0}^{n}\frac{1}{k!(n-k)!}\left(\frac{\beta r^2}{2}\right)^n\mathcal{S}^{4k-2n}\boldsymbol{\delta}.\end{aligned} \tag{29}$$

Since only the zeroth entry of $\boldsymbol{\delta}$ is nonzero and the shifting matrix $\mathcal{S}$ only appears with even exponents, all the odd-located elements of $\mathbf{Z}(r;\lambda)$ are zero, i.e.,

$$\{\mathbf{Z}(r;\lambda)\}^{2s+1} = 0. \tag{30}$$

As for the even elements, we have

$$\begin{aligned}\{\mathbf{Z}(r;\lambda)\}^{2s} &= e^{-\alpha r^2}\sum_{n=0}^{\infty}\sum_{k=0}^{n}\frac{1}{k!(n-k)!}\left(\frac{\beta r^2}{2}\right)^n\{\boldsymbol{\delta}\}^{2s+4k-2n}\\ &= e^{-\alpha r^2}\sum_{k=0}^{\infty}\sum_{n=k}^{\infty}\frac{1}{k!(n-k)!}\left(\frac{\beta r^2}{2}\right)^n\{\boldsymbol{\delta}\}^{2s+4k-2n}\\ &= e^{-\alpha r^2}\sum_{k=0}^{\infty}\frac{1}{k!(k+s)!}\left(\frac{\beta r^2}{2}\right)^{2k+2}\\ &= e^{-\alpha r^2}I_s(\beta r^2).\end{aligned} \tag{31}$$

In the first passage, the order of the two sums has been inverted. In the second one, the sum on n has been dropped since $\{\boldsymbol{\delta}\}^{2s+4k-2n}$ is nonzero iff $n=2k+s$. Finally, the Taylor expansion $I_s(z) = (z/2)^s\sum_{k=0}^{\infty}(z^2/4)^k/[k!(k+s)!]$ of the modified Bessel functions is used for $z=\beta r^2$.

From (24) and (30), we see that vector $\mathbf{Z}(r;\lambda)$ has all odd entries equal to zero, and all even entries proportional to the Bessel functions $I_s(\beta r^2)$, with a Gaussian factor $e^{-\alpha r^2}$. Therefore, by using vector $\mathbf{I}(z)$ defined in (24), with $z=\beta r^2$, expressions (30) and (31) can be collapsed into a single one, namely, $\mathbf{Z}(r;\lambda) = e^{-\alpha r^2}\mathbf{I}(\beta r^2)$. Finally, by plugging this expression into (26), (23) is obtained. ■

Remarks: In (23), $H_m(r\lambda\mathcal{R})H_n(r\lambda^{-1}I)$ is a polynomial of degree $m+n$ in matrices $\mathcal{S}$ and $\mathcal{S}^{-1}$, which we write as

$$H_m(\lambda r\mathcal{R})H_n(\lambda^{-1}rI) = \sum_{k=-(m+n)}^{m+n}P_{m,n}^k(\lambda r,\lambda^{-1}r)\mathcal{S}^k \tag{32}$$

where $P_{m,n}^k(u,v)$ is a polynomial of degree $m+n$ in u and v. Since matrix $\mathcal{S}^k$ shifts any vector of k positions, we conclude that term $U_{m,n}^s(r;\lambda)$ is the product of the Gaussian term $e^{-\alpha r^2}$ with a linear combination of modified Bessel functions of different orders, between $s-\lceil(m+n)/2\rceil$ and $s+\lceil(m+n)/2\rceil$, whose coefficients are expressed in terms of the Hermite coefficients and powers of λr and $\lambda^{-1}r$. Explicit expressions of functions $U_{m,n}^s(r;\lambda)$ are given in Table I for the orders zero,

TABLE I
RADIAL PARTS $U^s_{m,n}(r;\lambda)$ OF ORDERS ZERO, ONE, AND TWO

Functions $U^s_{m,n}(r,\lambda)$
$U^{2s}_{0,0}(r;\lambda) = e^{-\alpha r^2} I_s(\beta r^2)$
$U^{2s+1}_{0,0}(r;\lambda) = 0$
$U^{2s}_{1,0}(r;\lambda) = 0$
$U^{2s+1}_{1,0}(r;\lambda) = \lambda r e^{-\alpha r^2}[I_{s+1}(\beta r^2) + I_s(\beta r^2)]$
$U^{2s}_{0,1}(r;\lambda) = 0$
$U^{2s+1}_{0,1}(r;\lambda) = \frac{r}{\lambda i} e^{-\alpha r^2}[I_{s+1}(\beta r^2) - I_s(\beta r^2)]$
$U^{2s}_{2,0}(r;\lambda) = e^{-\alpha r^2}\left\{2\left(\lambda^2 r^2 - 1\right) I_s(\beta r^2) + \lambda^2 r^2 [I_{s+1}(\beta r^2) + I_{s-1}(\beta r^2)]\right\}$
$U^{2s+1}_{2,0}(r;\lambda) = 0$
$U^{2s}_{1,1}(r;\lambda) = \frac{r^2}{i} e^{-\alpha r^2}[I_{s+1}(\beta r^2) - I_{s-1}(\beta r^2)]$
$U^{2s+1}_{1,1}(r;\lambda) = 0$
$U^{2s}_{0,2}(r;\lambda) = e^{-\alpha r^2}\left\{2\left(\lambda^{-2} r^2 - 1\right) I_s(\beta r^2) - \lambda^{-2} r^2 [I_{s+1}(\beta r^2) + I_{s-1}(\beta r^2)]\right\}$
$U^{2s+1}_{0,2}(r;\lambda) = 0$

one, and two. As we see, the matrix form deployed in (23) considerably simplifies the notation and unifies the cases of even and odd indexes (m, n).

C. Recursive Formula for the Steering Functions

We now derive a recursive formula that enables computing the steering functions $V^s_{m,n}(\mathbf{r},\lambda)$ for every (m, n, s) without the need to evaluate Hermite polynomials of infinite matrices as in (23).

Theorem 3: The radial parts $V^s_{m,n}(\mathbf{r},\lambda)$ of the steering functions $V^s_{m,n}(\mathbf{r},\lambda)$ admit the following recursive formula:

$$U^s_{m+1,n}(r,\lambda) = \lambda r\left[U^{s-1}_{m,n}(r,\lambda) - U^{s+1}_{m,n}(r,\lambda)\right] - 2mU^s_{m,n}(r,\lambda) \quad (33)$$

$$U^s_{m,n+1}(r,\lambda) = \frac{r}{\lambda i}\left[U^{s-1}_{m,n}(r,\lambda) - U^{s+1}_{m,n}(r,\lambda)\right] - 2nU^s_{m,n}(r,\lambda). \quad (34)$$

Proof: By plugging into (23) the well-known identity $H_{p+1}(x) = 2xH_p(x) - 2pH_{n-1}(x)$ for the Hermite polynomials and using (13), we obtain

$$\begin{aligned}\mathbf{U}_{m+1,n}(r;\lambda) &= e^{-\alpha r^2} H_{m+1}(\lambda r\mathcal{R}) H_n(\lambda^{-1} rI)\mathbf{I}(\beta r^2)\\ &= e^{-\alpha r^2}\left[2\lambda r\mathcal{R}H_m(\lambda r\mathcal{R})H_n(\lambda^{-1}rI) - 2mH_{m-1}(\lambda r\mathcal{R})H_n(\lambda^{-1}rI)\right]\mathbf{I}(\beta r^2)\\ &= \lambda r(\mathcal{S}^{-1} + \mathcal{S})\mathbf{U}_{m,n}(r;\lambda) - 2m\mathbf{U}_{m-1,n}(r;\lambda)\end{aligned} \quad (35)$$

whose generic sth element writes as

$$U^s_{m+1,n}(r;\lambda) = \lambda r\left[U^{s-1}_{m,n}(r;\lambda) + U^{s+1}_{m,n}(r;\lambda)\right] - 2mU^s_{m-1,n}(r;\lambda) \quad (36)$$

thus proving (33). Identity (34) is similarly proved. ■

IV. FOURIER TRANSFORM OF THE STEERING BASES

In this section, we compute the 2-D Fourier transform of the steering functions $V^s_{m,n}(r,\theta;\lambda)$ previously defined. The sth Fourier harmonic of signal $x(\theta)$ will be indicated as follows:

$$\mathcal{F}_s\{x(\theta)\} \triangleq \frac{e^{is\theta}}{2\pi}\int_0^{2\pi} x(\varphi)e^{-is\varphi}d\varphi \quad (37)$$

Lemma 1: Let $T(\mathbf{r})$ be any summable function and $\tilde{T}(\boldsymbol{\omega}) = \mathcal{F}_{2D}\{T(\mathbf{r})\}$. Let $T_s(r)$ and $\tilde{T}_s(\rho)$ also be the sth coefficients of the Fourier expansions of $T(\mathbf{r})$ and $\tilde{T}(\boldsymbol{\omega})$ w.r.t. the angular coordinates θ and ϕ, respectively. Then, $\tilde{T}_s(\rho)e^{is\phi}$ is equal to the 2-D Fourier transform of $T(\mathbf{r})e^{is\theta}$, i.e.,

$$\begin{array}{ccc} T(\mathbf{r}) & \xrightarrow{\mathcal{F}_{2D}} & \tilde{T}(\boldsymbol{\omega}) \\ \downarrow \mathcal{F}_s & & \downarrow \mathcal{F}_s \\ T_s(r)e^{is\theta} & \xrightarrow{\mathcal{F}_{2D}} & \tilde{T}_s(\rho)e^{is\phi} \end{array}. \quad (38)$$

Proof: By definition, we have

$$\mathcal{F}_{2D}\{\mathcal{F}_s\{T(r,\theta)\}\}(\rho,\phi) = \frac{1}{2\pi}\int_0^{2\pi}\int_0^{2\pi}\int_0^{\infty} T(r,\alpha)e^{-in\alpha}e^{in\theta}e^{-ir\rho\cos(\theta-\phi)}r\mathrm{d}r\mathrm{d}\theta\mathrm{d}\alpha \quad (39)$$

$$\mathcal{F}_s\{\mathcal{F}_{2D}\{T(r,\theta)\}\}(\rho,\phi) = \frac{1}{2\pi}\int_0^{2\pi}\int_0^{2\pi}\int_0^{\infty} T(r,\theta)e^{-ir\rho\cos(\theta-\alpha)}e^{-in\alpha}e^{in\phi}r\mathrm{d}r\mathrm{d}\theta\mathrm{d}\alpha. \quad (40)$$

In (39), we evaluate the integral in $\mathrm{d}\theta$ by using the known result $(1/2\pi)\int_0^{2\pi} e^{in\theta - ir\rho\cos\theta}\mathrm{d}\theta = J_n(r\rho)$. With basic algebra, we get

$$\mathcal{F}_{2D}\{\mathcal{F}_s\{T(r,\theta)\}\}(\rho,\phi) = \int_0^{2\pi}\int_0^{\infty} T(r,\alpha)J_n(r\rho)e^{in(\phi-\alpha)}r\mathrm{d}r\mathrm{d}\alpha. \quad (41)$$

Similarly, in (40), we evaluate the integral in $\mathrm{d}\alpha$, thus obtaining

$$\mathcal{F}_{2D}\{\mathcal{F}_s\{T(r,\theta)\}\}(\rho,\phi) = \int_0^{2\pi}\int_0^{\infty} T(r,\theta)J_n(r\rho)e^{in(\phi-\theta)}r\mathrm{d}r\mathrm{d}\theta. \quad (42)$$

These two integrals coincide, thus proving the lemma. ■

Theorem 4: The following identity holds for the steering functions $V^s_{m,n}(\mathbf{r},\lambda)$:

$$V^s_{m,n}(\mathbf{r},\lambda) \xrightarrow{\mathcal{F}_{2D}} i^{m+n+s}V^s_{n,m}(\boldsymbol{\omega},\lambda). \quad (43)$$

Proof: Let's observe that

$$H_{m,n}(x,y;\lambda) = H_{n,m}(y,x;\lambda^{-1}) \quad (44)$$

which holds as a direct consequence of definition (10) of the elongated HGF. In other words, (44) implies that swapping vari-

able x and y is equivalent to swapping indexes m and n and replacing λ with λ^{-1}. Therefore, by noting that a variable swap persists in the frequency domain, expression (11) of the 2-D Fourier transform of $H_{m,n}(x,y,\lambda)$ can be written as

$$H_{m,n}(x,y,\lambda) \xrightarrow{\mathcal{F}_{2D}} i^{m+n} H_{n,m}(\eta,\xi;\lambda) \tag{45}$$

or, in polar coordinates

$$H_{m,n}(r\cos\theta, r\sin\theta;\lambda) \xrightarrow{\mathcal{F}_{2D}} i^{m+n} H_{n,m}(\rho\sin\phi, \rho\cos\phi;\lambda). \tag{46}$$

By posing $R_{m,n}(r,\theta;\lambda) \triangleq H_{m,n}(r\cos\theta, r\sin\theta;\lambda)$, (46) can be written as

$$R_{m,n}(r,\theta;\lambda) \xrightarrow{\mathcal{F}_{2D}} i^{m+n} R_{n,m}(\rho,\pi/2-\phi;\lambda). \tag{47}$$

We now compute, for both sides of (47), the sth harmonics of the Fourier expansion w.r.t. the angular coordinate. On the left-hand side, we get, by definition, $\mathcal{F}_s\{R_{m,n}(r,\theta;\lambda)\} = V^s_{m,n}(\rho,\phi;\lambda) = U^s_{m,n}(r;\lambda)e^{is\theta}$. On the right-hand side, we get $\mathcal{F}_s\{R_{m,n}(r,\pi/2-\theta;\lambda)\} = i^s V^s_{n,m}(\rho,\phi;\lambda) = i^s U^s_{m,n}(\rho;\lambda)e^{is\phi}$, where factor i^s comes from the fact that the value of the angular coordinate is $\pi/2-\phi$ instead of ϕ, i.e.,

$$\begin{array}{ccc} R_{m,n}(r,\theta;\lambda) & \xrightarrow{\mathcal{F}_{2D}} & i^{m+n} R_{n,m}(\rho,\pi/2-\phi;\lambda) \\ \downarrow \mathcal{F}_s & & \downarrow \mathcal{F}_s \\ U^s_{m,n}(r;\lambda)e^{is\theta} & & i^{m+n+s} U^s_{m,n}(\rho;\lambda)e^{is\phi} \end{array}. \tag{48}$$

Thus, given Lemma 1, we can write

$$U^s_{m,n}(r;\lambda)e^{is\theta} \xrightarrow{\mathcal{F}_{2D}} i^{m+n+s} U^s_{m,n}(\rho;\lambda)e^{is\phi} \tag{49}$$

thus proving (43). ■

Remarks: The two sides of (43) only differ for the order of m and n. Therefore, for $m = n$, functions $V^s_{m,n}(r,\theta;\lambda)$ are eigenfunctions of the 2-D Fourier transform, with eigenvalues i^{2n+s}. This is not trivial since the elongated HGFs, from which $V^s_{m,n}(r,\theta;\lambda)$ are derived, are *not* Fourier eigenfunctions.

As a corollary of this result, we observe that functions $U^s_{m,n}(r;\lambda)$ are eigenfunctions of the sth-order Hankel transform for $m = n$. This is a direct consequence of the well-known fact that the 2-D Fourier transform of a CHF is still a CHF, whose radial part is the sth-order Hankel transform of the radial part of the original CHF. More precisely, we have

$$\int_0^\infty U^s_{m,n}(r;\lambda) J_s(r\rho) r\mathrm{d}r = i^{m+n+s} U^s_{m,n}(\rho;\lambda) \tag{50}$$

where $J_s(z)$ is the Bessel function of the first kind.

V. Application

Although the main contribution of this paper is theoretical, an application of the proposed filters to gradient estimation of natural images is discussed in this section.

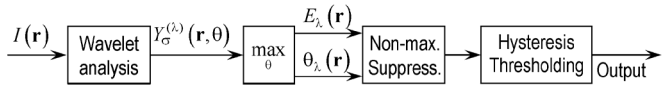

Fig. 7. Edge detection scheme.

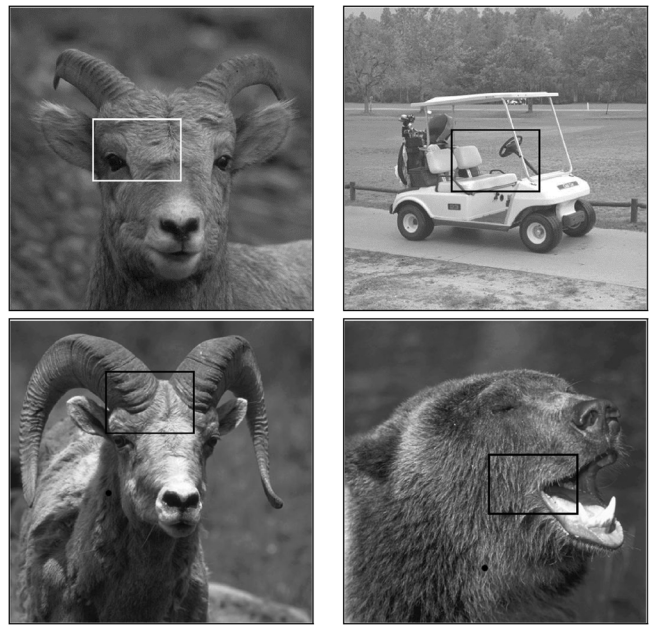

Fig. 8. Four test images for the proposed application. (Rectangles) Cropped areas detailed in Figs. 9 and 10.

Estimating the gradient of a given image is an important computational step in many image processing and pattern recognition tasks, such as contour detection and image segmentation [4], [33]–[35], active contours [36]–[38], denoising [39], image classification [40], image alignment [41], watermarking [42], [43], and biomedical imaging [44], [45], just to cite a few. The main difficulty when computing the gradient of an image is that, as well known, it is an ill-posed problem, as infinitesimal perturbations of the input image may produce large variations of its gradient. Therefore, several regularization techniques have been developed to reliably estimate the image gradient (see, e.g., [35] for a survey) and the subject is still a fertile area of ongoing research [46], [47]. The classical approach to estimate the gradient is to convolve the input with the gradient of an isotropic Gaussian kernel [4]. However, as discussed in Section I, it results in low orientation selectivity and a poor compromise between noise rejection versus accuracy in edge position. In contrast, we use the first derivative of an elongated Gaussian kernel.

Specifically, we follow the widely adopted scheme of Fig. 7, where the block "Wavelet analysis" is detailed in Fig. 5. First, the input image is convolved with the proposed CHF $V^s_{(0,1)}(\mathbf{r}/\sigma,\lambda)$ of order $(m,n) = (0,1)$, where σ is a scale parameter. The analytical expression of the radial part of these CHFs is given in the third row of Table I. The output $Y^\lambda_\sigma(\mathbf{r},\theta)$ of the block "Wavelet analysis" defined in (2) is the best approximation of the convolution of the input image with the elongated HGF $H_{0,1}(R_\theta\mathbf{r}/\sigma;\lambda)$. As discussed in Section II-B, this filter estimates the gradient better than an isotropic HGF.

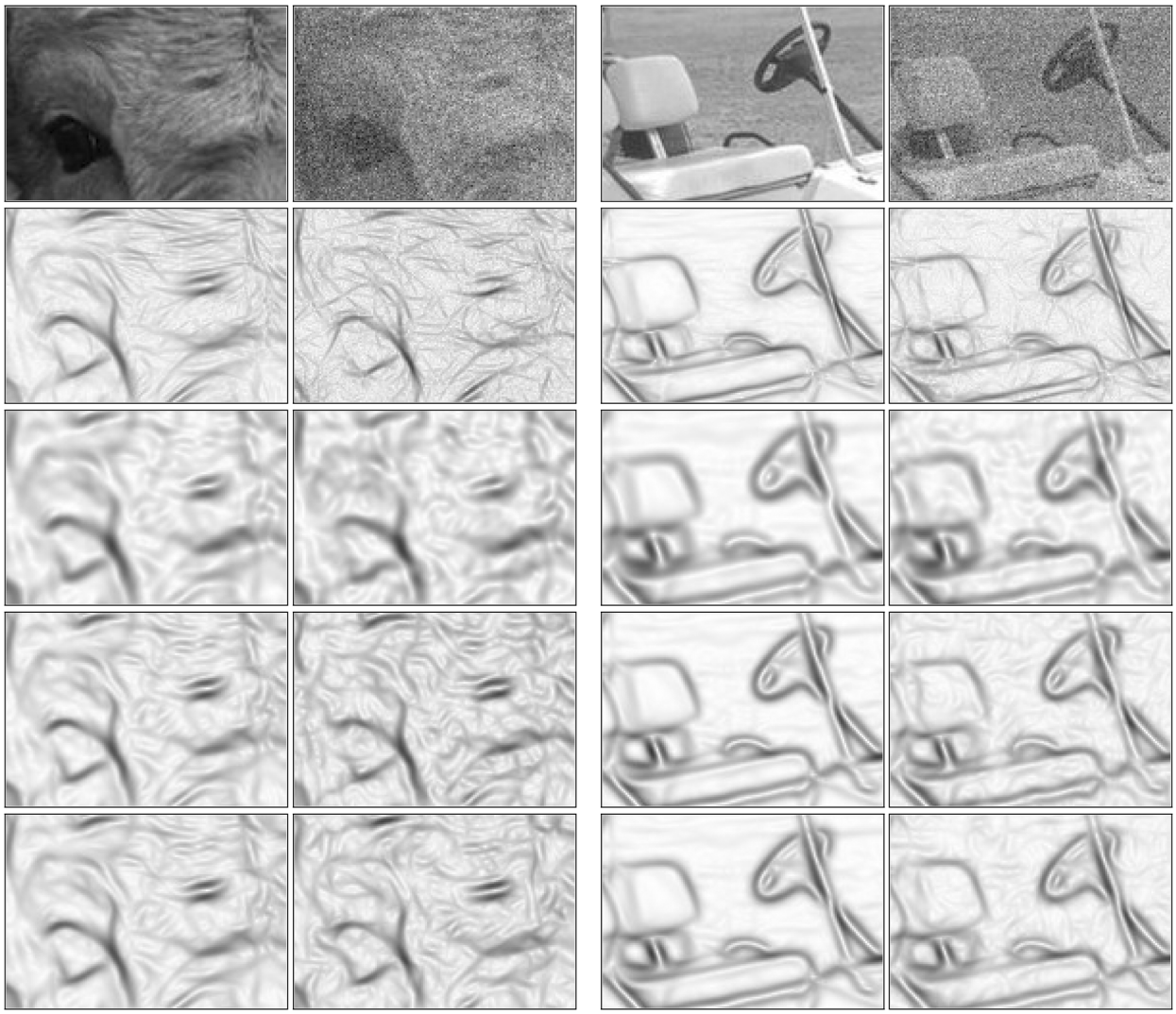

Fig. 9. Comparison of different steerable filters for gradient estimation. First row: Input images, both noise-free and corrupted with additive uncorrelated Gaussian noise (SNR = 10 dB). Second row: Output of the proposed operator, for $\lambda^2 = 8$. Third row: Isotropic Gaussian gradient. Fourth and fifth rows: Outputs of the anisotropic steerable filters proposed in [17]. and [11], respectively. For all filters, the scale parameter has been chosen to have the same noise rejection. The filters proposed here reach the best localization.

To detect edges, we compute the local edge direction $\theta_{\lambda,\sigma}(\mathbf{r})$ and the local edge strength $E_{\lambda,\sigma}(\mathbf{r})$ as

$$\theta_{\lambda,\sigma}(\mathbf{r}) \triangleq \arg\max_{\theta} Y_{\sigma}^{\lambda}(\mathbf{r},\theta) \qquad E_{\lambda,\sigma}(\mathbf{r}) = Y_{\sigma}^{\lambda}\left[\mathbf{r},\theta_{\lambda,\sigma}(\mathbf{r})\right]. \tag{51}$$

The amount of smoothing that is made by this filter is $\lambda\sigma$ along the edge and $\lambda^{-1}\sigma$ across the edge. The amount of noise that is filtered out, which is proportional to the product of the two scale parameters in the two orthogonal directions, does not depend on λ but on σ only.

We now show and discuss some experimental results related to the use of the proposed wavelets for gradient estimation. We compare the outputs of our filters for $\lambda^2 = 8$ both with the classic isotropic gradient [4] and with two other recently introduced anisotropic steerable filters, namely, a Canny-optimal steerable filter [17] and a filter based on complex Gaussian derivatives [11]. All methods have been tested on a set of 40 images (512 × 512 pixels), both noise-free and corrupted by additive uncorrelated Gaussian noise (SNR = 10 dB), with the same values of the input parameters. In particular, the value of the scale parameter has been adjusted to have the same level of noise rejection in all filtered images.

For the input images of Fig. 8, results are shown in Figs. 9 and 10, where crops are displayed to highlight the performances of the considered filters at a higher level of detail. The entire set of examples, with full images, is available online.[1] As we see, the proposed filters outperform all other studied methods in terms of better rendering of both contours and texture details, particularly for elongated structures.

1) For the same amount of noise rejection, contours are better localized because of the smaller smoothing across the edge direction. This is particularly evident in the presence of pairs of junctions, such as at the crossing between two differently oriented thin structures in the golfcart in Fig. 9. As we see, with standard isotropic filters, the contours of the bars in the golfcart are deformed, whereas elongated filters do not give rise to similar artifacts.

[1]http://www.comlab.uniroma3.it/steerable.html

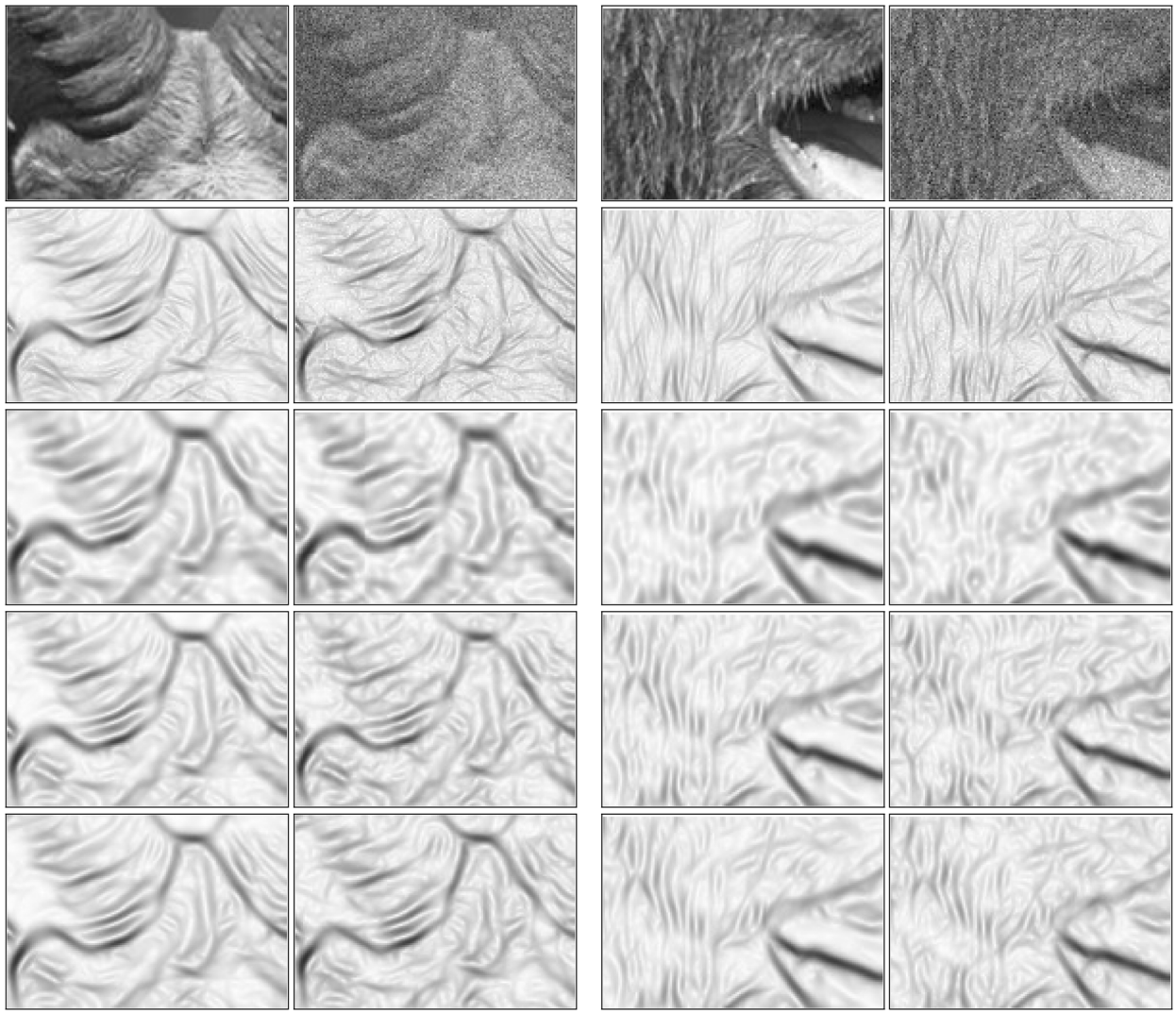

Fig. 10. Same as Fig. 9 for other input images.

2) The proposed elongated filter is more robust to contour fragmentation due to larger smoothing along the edge direction.
3) The proposed filter better renders elongated directional texture than the classical isotropic one. This can be seen particularly well, e.g., in the fur of the goat, in which elongated filters give rise to structured chains of collinear edges, instead of meaningless random patterns as that with the nonelongated convolution kernels.

To quantify the performance of the proposed approach, we compute binary edge maps from $E_{\lambda,\sigma}(\mathbf{r})$ as in [4], and we measure their similarity to manually drawn ground truths. Binarization is performed by standard nonmaxima suppression and hysteresis thresholding, where the value of the high threshold is adaptively computed for each image by imposing that fraction p of pixels above the threshold is constant. The similarity between a binary edge map $b(\mathbf{r})$ and the ground truth $b_{\mathrm{GT}}(\mathbf{r})$ is measured by means of the well-established Pratt figure of merit F [48], which is defined as

$$F = \frac{1}{\max\left\{\sum_{\mathbf{r}} b(\mathbf{r}), \sum_{\mathbf{r}} b_{\mathrm{GT}}(\mathbf{r})\right\}} \sum_{\mathbf{r}} \frac{b(\mathbf{r})}{1 + \frac{d^2_{\mathrm{GT}}(\mathbf{r})}{\sigma^2_{err}}} \tag{52}$$

where $d_{\mathrm{GT}}(\mathbf{r})$ is the distance transform of $b_{\mathrm{GT}}(\mathbf{r})$ and σ_{err} is the uncertainty in the position of an edge in the ground truth, arising to the fact that it is drawn by hand. We used value $\sigma_{err} = 1$. The figure of merit F is always comprised between 0 and 1, being 1 iff the detected contours coincide with the ground truth.

The values of F, averaged over a set of 40 images, are plotted versus p in Fig. 11(a) for different values of λ. This graph shows two facts. First, as λ increases, the maximum value $F_{\max}$ of F increases, thus showing an improvement of about 12.5% w.r.t. isotropic filters. Second, as λ increases, the optimal value of p gets closer to the average fraction of edge pixels in the ground truths.

A study of the influence of the scale parameter σ on the performance has been also carried out. In particular, value $F_{\max}$, which is obtained after optimizing the edge detector w.r.t. p, is plotted versus σ in Fig. 11(b) for different elongations λ. The local maxima correspond to the best compromise between high edge localization (low σ) and high noise rejection (high σ). As we see, higher elongation leads to better performance and higher values of the optimal σ, which means that a large amount of noise can be removed. In particular, in Fig. 12, we show the average and the standard deviation of the values of F over the entire data set. As we see, the proposed wavelets outperform both classical

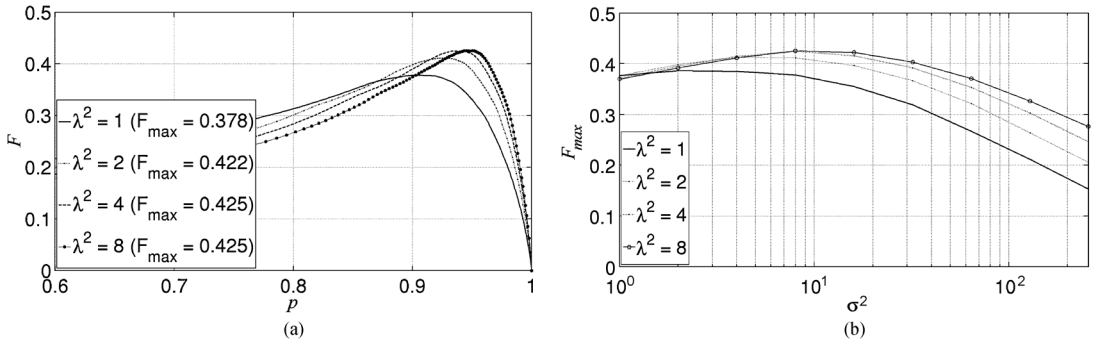

Fig. 11. Quantitative performance evaluation of the proposed edge detector. (a) Performance of the proposed method, averaged on a set of 40 images, for different values of λ and with constant $\sigma = 2$, plotted versus the fraction of pixels that are below the threshold. (b) Performance at varying σ for different values of λ after optimizing the threshold on the entire data set.

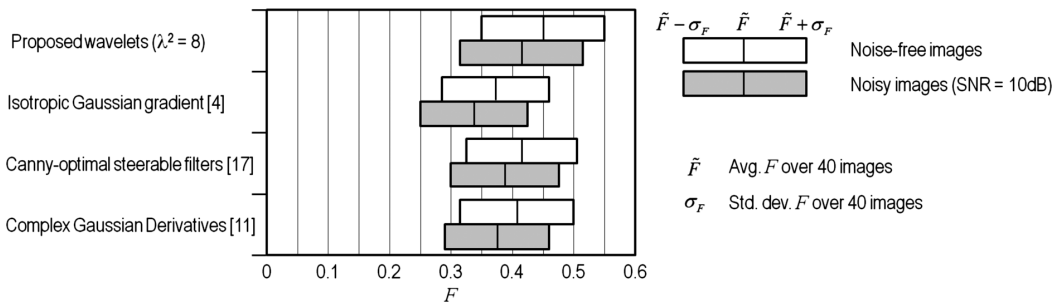

Fig. 12. Robustness to noise of the filters studied here. For each considered filter, statistics of their performances on the entire data set of 40 images are shown both for noise-free and noisy images (SNR $= 10$ dB), after individually optimizing their input parameters, which have been kept constant across the entire input data set. The proposed filters outperform both classic isotropic and more recently introduced anisotropic filters.

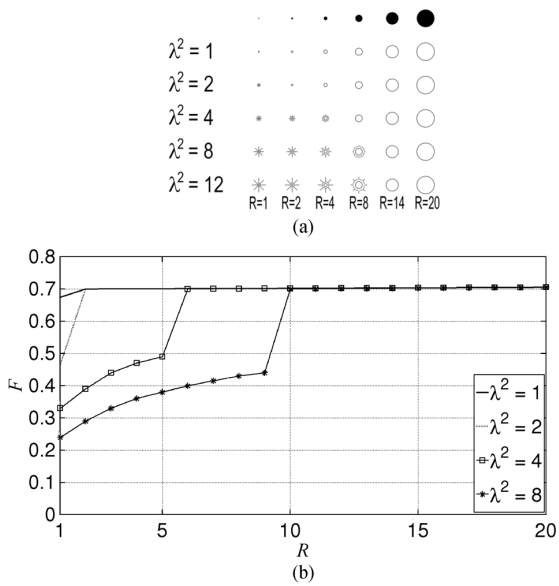

Fig. 13. Behavior of the studied filters in presence of high curvature points. (a) Synthetic input images and edges detected with several values of λ. (b) Edge detection performance in terms of F at varying R. As we see, there are no artifacts for $R > \lambda^2$.

Gaussian gradient and more recently introduced anisotropic steerable filters, both for noise-free and noisy images.

Finally, the behavior of the proposed filters in the presence of high curvature points, which is a particularly critical situation for elongated filters, has been studied. Specifically, synthetic images, which consist of disks of radius R between 1 and 20 pixels [see Fig. 13(a)], have been constructed. Their ground truth can be easily obtained. The proposed method has been applied to such images for different elongations λ, by keeping constant the width of the filters in the direction across the edge (i.e., same position accuracy), so that the amount of smoothing along the edge direction increases as λ increases.

The resulting edge maps are shown in Fig. 13(a). As we see, elongated filters result in several artifacts when the curvature radius R is lower than λ^2. To quantify the effect of such artifacts on the edge-detection performance, the dissimilarity of the ground truths has been measured in terms of the figure of merit F previously defined. Results, displayed in [see Fig. 13(b)], show that artifacts disappear when the curvature radius of the detected edge is greater than λ^2.

VI. Summary and Conclusion

A new family of eigenfunctions of the 2-D Fourier transform has been presented. In particular, an analytical expression for the steering functions $V^s_{m,n}(\mathbf{r}, \lambda)$ of the elongated HGFs is provided both in the spatial and frequency domains, making use of a Gaussian term, modified Bessel functions, Hermite polynomials, and complex exponentials. While the analytical expressions of Table I are rather complicated, the matrix notation here introduced results in the much more treatable expression (23), in which the cases of odd and even orders of the Hermite polynomials are unified. This enables us to more deeply study their mathematical properties, thus leading to a more solid and rigorous theoretical background to build future applications upon. In particular, a recursive formula for the new wavelets has been also derived, which allows a more efficient implementation. Moreover, it has been shown that these filters give rise to a

new dyadic family of the 2-D Fourier transform. The latter result is nontrivial since the *elongated* HGFs, from which the new wavelets are derived, are *not* Fourier eigenfunctions.

The new steering functions $V^s_{m,n}(\mathbf{r}, \lambda)$ are a natural generalization of the well-known Laguerre–Gauss harmonics [49], to which they reduce for $\lambda = 1$. This is a direct consequence of the fact that, for $\lambda = 1$, functions $V^s_{m,n}(\mathbf{r}, \lambda)$ become the steering functions of the isotropic HGF [2]. Consequently, we expect the new wavelets to be useful in all areas of image processing in which the Laguerre–Gauss harmonics have been applied with success. Examples are texture modeling, classification, stereoscopic imaging, denoising, and image and video compression just to cite a few.

The new wavelets of order $(m, n) = (0, 1)$ have been used for gradient estimation. Although the presented application is only illustrative, results are promising and show the potentiality of the new wavelets to improve the Canny limit in the tradeoff between noise rejection and localization accuracy. In particular, qualitative and quantitative comparisons with existing both isotropic and more recently introduced anisotropic methods [11], [17] show the capability of the new filters to perform better feature extraction, both for edge detection and texture modeling. Quantitatively, the new wavelets improve the edge-detection performance of about 12.5% with respect to standard methods, in terms of the Pratt figure of merit.

The usage of steered derivatives of an elongated Gaussian kernel for oriented feature extraction was already proposed in [13]. However, only the orders zero, one, and two were considered, and only numerical approximations of the steering functions were presented. In contrast, a compact analytical form has been presented here, along with several mathematical properties of the steering functions.

In particular, the fact that the new wavelets give rise to a new set of Fourier eigenfunctions makes them interesting for some other signal and image processing areas, such as joint time–frequency analysis [50], as well as for other fields of science, such as optics and quantum mechanics.

REFERENCES

[1] S. G. Mallat, "A theory for multiresolution signal decomposition: The wavelet representation," *IEEE Trans. Pattern Anal. Mach. Intell.*, vol. 11, no. 7, pp. 674–693, Jul. 1989.

[2] I. Kimel and L. R. Elias, "Relations between Hermite and Laguerre Gaussian modes," *IEEE J. Quantum Electron.*, vol. 29, no. 9, pp. 2562–2567, Sep. 1993.

[3] J. L. Silván-Cárdenas and B. Escalante-Ramirez, "The multiscale Hermite transform for local orientation analysis," *IEEE Trans. Image Process.*, vol. 15, no. 5, pp. 1236–1253, May 2006.

[4] J. F. Canny, "A computational approach to edge detection," *IEEE Trans. Pattern Anal. Mach. Intell.*, vol. PAMI-8, no. 6, pp. 679–698, Nov. 1986.

[5] A. L. Yuille and T. A. Poggio, "Scaling theorems for zero crossings," *IEEE Trans. Pattern Anal. Mach. Intell.*, vol. PAMI-8, no. 1, pp. 15–25, Jan. 1986.

[6] M. Bertero, T. A. Poggio, and V. Torre, "Ill-posed problems in early vision," *Proc. IEEE*, vol. 76, no. 8, pp. 869–889, Aug. 1988.

[7] B. M. ter Haar Romeny, *Geometry-Driven Diffusion in Computer Vision*. Norwell, MA: Kluwer, Sep. 1994.

[8] S. M. M. Rahman, M. O. Ahmad, and M. N. S. Swamy, "Wavelet-based video denoising using gauss-Hermite density function," in *Proc. IEEE MWSCAS*, 2006, vol. 1, pp. 592–595.

[9] A. Refregier, "Shapelets—I. A method for image analysis," *Month. Not. Royal Astr. Soc.*, vol. 338, no. 1, pp. 35–47, Jan. 2003.

[10] R. Massey and A. Refregier, "Polar shapelets," *Month. Not. Royal Astr. Soc.*, vol. 363, no. 1, pp. 197–210, 2005.

[11] M. Reisert and H. Burkhardt, "Complex derivative filters," *IEEE Trans. Image Process.*, vol. 17, no. 12, pp. 2265–2274, Dec. 2008.

[12] P. Perona, "Steerable-scalable kernels for edge detection and junction analysis," *Image Vis. Comput.*, vol. 10, no. 10, pp. 663–672, Dec. 1992.

[13] P. Perona, "Deformable kernels for early vision," *IEEE Trans. Pattern Anal. Mach. Intell.*, vol. 17, no. 5, pp. 488–499, May 1995.

[14] E. P. Simoncelli and H. Farid, "Steerable wedge filters for local orientation analysis," *IEEE Trans. Image Process.*, vol. 5, no. 9, pp. 1377–1382, Sep. 1996.

[15] R. Manduchi, P. Perona, and D. Shy, "Efficient deformable filter banks," *IEEE Trans. Signal Process.*, vol. 46, no. 4, pp. 1168–1173, Apr. 1998.

[16] S. Berlemont and J. C. Olivo-Marin, "Combining local filtering and multiscale analysis for edge, ridge, and curvilinear objects detection," *IEEE Trans. Image Process.*, vol. 19, no. 1, pp. 74–84, Jan. 2010.

[17] M. Jacob and M. Unser, "Design of steerable filters for feature detection using Canny-like criteria," *IEEE Trans. Pattern Anal. Mach. Intell.*, vol. 26, no. 8, pp. 1007–1019, Aug. 2004.

[18] G. Papari and N. Petkov, "An improved model for surround suppression by steerable filters and multilevel inhibition with application to contour detection," *Pattern Recognit.*, vol. 44, no. 9, pp. 1999–2007, Sep. 2011.

[19] D. Charalampidis, "Steerable weighted median filters," *IEEE Trans. Image Process.*, vol. 19, no. 4, pp. 882–894, Apr. 2010.

[20] M. N. Do and M. Vetterli, "Rotation invariant texture characterization and retrieval using steerable wavelet-domain hidden Markov models," *IEEE Trans. Multimedia*, vol. 4, no. 4, pp. 517–527, Dec. 2002.

[21] J. Portilla, V. Strela, M. J. Wainwright, and E. P. Simoncelli, "Image denoising using scale mixtures of Gaussians in the wavelet domain," *IEEE Trans. Image Process.*, vol. 12, no. 11, pp. 1338–1351, Nov. 2003.

[22] A. Bharath and J. Ng, "A steerable complex wavelet construction and its application to image denoising," *IEEE Trans. Image Process.*, vol. 14, no. 7, pp. 948–959, Jul. 2005.

[23] X. Shi, A. L. R. Castro, R. Manduchi, and R. Montgomery, "Rotational invariant operators based on steerable filter banks," *IEEE Signal Process. Lett.*, vol. 13, no. 11, pp. 684–687, Nov. 2006.

[24] E. P. Simoncelli, W. T. Freeman, E. H. Adelson, and D. J. Heeger, "Shiftable multiscale transforms," *IEEE Trans. Inf. Theory*, vol. 38, no. 2, pp. 587–607, Mar. 1992.

[25] A. Karasaridis and E. Simoncelli, "A filter design technique for steerable pyramid image transforms," in *Conf. Proc. IEEE ICASSP*, 1996, vol. 4, pp. 2387–2390.

[26] G. Papari, P. Campisi, and N. Petkov, "Steerable filtering using novel circular harmonic functions with application to edge detection," in *Proc. Int. Conf. Pattern Recognit.*, 2010, pp. 3947–3950.

[27] G. Sommer, M. Michaelis, and R. Herpers, "The SVD approach for steerable filter design," in *Proc. IEEE Int. Symp. Circuits Syst.*, 1998, vol. 5, pp. 349–353.

[28] P. C. Teo and Y. Hel-Or, "Design of multiparameter steerable functions using cascade basis reduction," *IEEE Trans. Pattern Anal. Mach. Intell.*, vol. 21, no. 6, pp. 552–556, Jun. 1999.

[29] W. T. Freeman and E. H. Adelson, "The design and use of steerable filters," *IEEE Trans. Pattern Anal. Mach. Intell.*, vol. 13, no. 9, pp. 891–906, Sep. 1991.

[30] K. Mikolajczyk and C. Schmid, "A performance evaluation of local descriptors," *IEEE Trans. Pattern Anal. Mach. Intell.*, vol. 27, no. 10, pp. 1615–1630, Oct. 2005.

[31] M. Michaelis and G. Sommer, "A lie group approach to steerable filters," *Pattern Recognit. Lett.*, vol. 16, no. 11, pp. 1165–1174, Nov. 1995.

[32] D. Shy and P. Perona, "X-Y separable pyramid steerable scalable kernels," in *Proc. IEEE CVPR*, 1994, pp. 237–244.

[33] D. R. Martin, C. Fowlkes, and J. Malik, "Learning to detect natural image boundaries using local brightness, color, and texture cues," *IEEE Trans. Pattern Anal. Mach. Intell.*, vol. 26, no. 5, pp. 530–549, May 2004.

[34] G. Papari and N. Petkov, "Adaptive pseudo-dilation for gestalt edge grouping and contour detection," *IEEE Trans. Image Process.*, vol. 17, no. 10, pp. 1950–1962, Oct. 2008.

[35] G. Papari and N. Petkov, "Edge and line oriented contour detection: State of the art," *Image Vis. Comput.*, vol. 29, no. 2/3, pp. 79–103, 2011.

[36] N. Paragios, O. Mellina-Gottardo, and V. Ramesh, "Gradient vector flow fast geometric active contours," *IEEE Trans. Pattern Anal. Mach. Intell.*, vol. 26, no. 3, pp. 402–407, Mar. 2004.

[37] O. Michailovich, Y. Rathi, and A. Tannenbaum, "Image segmentation using active contours driven by the bhattacharyya gradient flow," *IEEE Trans. Image Process.*, vol. 16, no. 11, pp. 2787–2801, Nov. 2007.

[38] X. Xie, "Active contouring based on gradient vector interaction and constrained level set diffusion," *IEEE Trans. Image Process.*, vol. 19, no. 1, pp. 154–164, Jan. 2010.

[39] A. Beck and M. Teboulle, "Fast gradient-based algorithms for constrained total variation image denoising and deblurring problems," *IEEE Trans. Image Process.*, vol. 18, no. 11, pp. 2419–2434, Nov. 2009.

[40] N. R. Mudigonda, R. Rangayyan, and J. E. L. Desautels, "Gradient and texture analysis for the classification of mammographic masses," *IEEE Trans. Med. Imag.*, vol. 19, no. 10, pp. 1032–1043, Oct. 2000.
[41] R. Mégret, J. Authesserre, and Y. Berthoumieu, "Bidirectional composition on lie groups for gradient-based image alignment," *IEEE Trans. Image Process.*, vol. 19, no. 9, pp. 2369–2381, Sep. 2010.
[42] F. Yanbin, C. Wenyong, and P. Zhenkuan, "An adaptive watermarking algorithm in DWT domain based on multi-scale morphological gradient," in *Proc. IEEE Int. Conf. Comput. Sci. Softw. Eng.*, 2008, vol. 3, pp. 738–741.
[43] E. Nezhadarya, Z. Wang, and R. Ward, "Robust image watermarking based on multiscale gradient direction quantization," *IEEE Trans. Inf. Forensics Security*, vol. 6, no. 4, pp. 1200–1213, Dec. 2011.
[44] Q. Li, E. Asma, S. Ahn, and R. M. Leahy, "A fast fully 4-d incremental gradient reconstruction algorithm for list mode pet data," *IEEE Trans. Med. Imag.*, vol. 26, no. 1, pp. 58–67, Jan. 2007.
[45] P. Markelj, D. Tomazevic, F. Pernus, and B. Likar, "Robust gradient-based 3-D/2-D registration of CT and MR to X-ray images," *IEEE Trans. Med. Imag.*, vol. 27, no. 12, pp. 1704–1714, Dec. 2008.
[46] H. G. Senel, "Gradient estimation using wide support operators," *IEEE Trans. Image Process.*, vol. 18, no. 4, pp. 867–878, Apr. 2009.
[47] E. Nezhadarya and R. Ward, "A new scheme for robust gradient vector estimation in color images," *IEEE Trans. Image Process.*, vol. 20, no. 8, pp. 2211–2220, Aug. 2011.
[48] I. E. Abdou and W. K. Pratt, "Quantitative design and evaluation of enhancement/thresholding edge detectors," *Proc. IEEE*, vol. 67, no. 5, pp. 753–763, May 1979.
[49] G. Jacovitti and A. Neri, "Multiresolution circular harmonic decomposition," *IEEE Trans. Signal Process.*, vol. 48, no. 11, pp. 3242–3247, Nov. 2000.
[50] L. Cohen, *Time-Frequency Analysis: Theory and Applications*. Englewood Cliffs, NJ: Prentice-Hall, 1995.

Giuseppe Papari (M'10) was born in Rome, Italy, in 1979. He received the M.S. degree (*cum laude*) in electrical engineering from the University of Roma Tre, Roma, Italy, in 2003 and the Ph.D. degree (*cum laude*) in computing science from the University of Groningen, Groningen, The Netherlands, in 2009.

He was a Postdoc in computing science with the Universities of Groningen and Leiden, The Netherlands. He is currently a Postdoctoral Researcher in image analysis with the National Institute of Research in Informatics and Automatics, Rocquencourt, France. He has published more than 20 papers about Fourier analysis, contour detection, perceptual grouping, painterly rendering, and multiresolution analysis, one of which was invited to the IEEE international conference on computers and devices for communications in 2006. His main research interests are nonlinear filtering, contour detection, image segmentation, multiresolution analysis, clustering, pattern recognition, and morphological analysis.

Dr. Papari received two European Research Consortium for Informatics and Mathematics Alain Bensoussan Fellowships in 2011 and 2012 and one of the four IBM Best Student Paper Awards at the IEEE International Conference on Image Processing in 2006.

Patrizio Campisi (M'00–SM'08) received the Ph.D. degree in electrical engineering from the Università degli Studi "Roma Tre," Roma, Italy.

He is a Professor in telecommunications with the Department of Applied Electronics Università degli Studi "Roma Tre." He is a Coeditor of the book "Blind Image Deconvolution: Theory and Applications," CRC press, Boca Raton, FL, May 2007. His research interests are in the area of secure multimedia communications and multimedia forensics. Specifically, he has been working on secure biometric recognition, digital watermarking, image deconvolution, image analysis, stereo image and video processing, blind equalization of data signals, and secure communications.

Dr. Campisi is the Technical Program Cochair of the IEEE Workshop on Information Forensics and Security 2012. He was the General Chair of the 12th Association for Computing Machinery Workshop on Multimedia and Security, September 9–10, 2010, in Rome, Italy. He is a corecipient of the IEEE International Conference on Image Processing 2006 and IEEE International Conference on Biometrics: Theory, Applications, and Systems 2008 best student paper awards and of an IEEE Biometric Symposium 2007 best paper award. He is an Associate Editor of IEEE SIGNAL PROCESSING LETTERS (2008–2012). He is also Associate Editor for IEEE Transaction on Information Forensics and Security (2012–2015). He is an Elected Member of the IEEE Information Forensics and Security Technical Committee (2011–2013). Since 2007, he has been a member of the IEEE Certified Biometric Program Learning System Committee and of the IEEE Technical Committee on Information Assurance and Intelligent Multimedia—Mobile Communications, System, Man, and Cybernetics Society. He is an Associate Editor of the IET Biometrics. Since 2009, he has been an Associate Editor of the *International Journal of Digital Crime and Forensics* and of the *Advances in Multimedia by Hindawi*.

Nicolai Petkov received the Dr.sc.techn. degree in computer engineering (Informationstechnik) from Dresden University of Technology, Dresden, Germany.

In 1989, he was awarded an Alexander von Humboldt scholarship of the Federal Republic of Germany. In 1991, he held research positions with the University of Wuppertal, Wuppertal, Germany; the University of Erlangen-Nürnberg, Erlangen, Germany; the Academy of Sciences in Berlin, Germany; and Dresden University of Technology. He is a Professor of computer science and the Head of the Research Institute of Mathematics and Computing Science, University of Groningen, Groningen, The Netherlands. He is the author of two monographs and (co)author of another book, four patents, and over 100 scientific papers. He is a member of the editorial boards of several journals. His current research focuses on computer simulations and understanding of the visual system of the brain and using the obtained insights for the development of effective computer vision algorithms. He is also interested in using computers for artistic expression.